

Article

Indigo Carmine Degradation in Water Induced by a Pulsed Positive Corona Discharge in Air: Discharge and Postdischarge Effects

Matías G. Ferreyra ^{1,*} , Brenda L. Fina ¹, Natalio J. Milardovich ¹, Juan C. Chamorro ¹, Brenda Santamaría ¹, Karina Balestrasse ² and Leandro Prevosto ¹

¹ Grupo de Descargas Eléctricas (GDE), Departamento Ing. Electromecánica, Facultad Regional Venado Tuerto, Universidad Tecnológica Nacional, Consejo Nacional de Investigaciones Científicas y Técnicas (CONICET), Laprida 651, Venado Tuerto S2600, Argentina; brendafina@gmail.com (B.L.F.); nmilardovich@gmail.com (N.J.M.); jcchamorro@utp.edu.co (J.C.C.); brendasantamaria1989@gmail.com (B.S.); prevosto@waycom.com.ar (L.P.)

² Instituto de Investigaciones en Biociencias Agrícolas y Ambientales (INBA), Facultad de Agronomía, Universidad de Buenos Aires, CONICET, San Martín 4453, Ciudad Autónoma de Buenos Aires C1417DSE, Argentina; kbale@agro.uba.ar

* Correspondence: matiasg.ferreyra@hotmail.com

Abstract: In recent years, one of the fastest growing technological applications in the field of nonthermal plasmas is the degradation of organic contaminants of water. In this work, the degradation of indigo carmine (IC) in water induced by a pulsed positive corona discharge operating in ambient air is reported. Degradation levels in different volumes of IC in solution with distilled water treated with different plasma exposure times immediately after discharge (0 h), and in the postdischarge up to 24 h were examined. To explain the IC discoloration in the postdischarge phase, a chemical model was developed. The stability of the reactive species in solution nitrate (NO_3^-), nitrite (NO_2^-) and hydrogen peroxide (H_2O_2), as well as the properties of the solution (electrical conductivity, pH) were also measured. The results suggest that the hydroxyl radical (OH^\cdot) as well as ozone (O_3) are the main oxidizing species during the discharge phase, being primarily formed in the gas phase through plasma-mediated reactions and then transferred to the liquid by diffusion, while the OH^\cdot production in the bulk liquid through the decomposition of peroxynitrous acid ($\text{O}=\text{NOOH}$) plays a major role in the IC degradation during the postdischarge. These results are associated with a noticeably increase in the energy-yield values observed at 24 h post-treatment.

Keywords: nonthermal plasma; indigo carmine degradation; pulsed corona discharge; postdischarge effects; reactive species in water



Citation: Ferreyra, M.G.; Fina, B.L.; Milardovich, N.J.; Chamorro, J.C.; Santamaría, B.; Balestrasse, K.; Prevosto, L. Indigo Carmine Degradation in Water Induced by a Pulsed Positive Corona Discharge in Air: Discharge and Postdischarge Effects. *Plasma* **2022**, *5*, 265–279. <https://doi.org/10.3390/plasma5020021>

Academic Editor: Andrey Starikovskiy

Received: 3 May 2022

Accepted: 27 May 2022

Published: 30 May 2022

Publisher's Note: MDPI stays neutral with regard to jurisdictional claims in published maps and institutional affiliations.



Copyright: © 2022 by the authors. Licensee MDPI, Basel, Switzerland. This article is an open access article distributed under the terms and conditions of the Creative Commons Attribution (CC BY) license (<https://creativecommons.org/licenses/by/4.0/>).

1. Introduction

A plasma is a quasineutral gas of charged and neutral particles that exhibits collective behavior [1]. On a laboratory scale, the most usual mode of plasma generation is through electrical discharges in a gaseous medium [2]. These are usually divided into two broad categories: (i) thermal discharges, where the energies of the heavy particles are of the order of the electron energy ($\sim 1 \text{ eV} = 11,600 \text{ K}$) [3]; and (ii) nonthermal discharges, where the electron energy is much higher ($\sim 1\text{--}5 \text{ eV}$) than the energy of the heavy particles ($\sim 300\text{--}3000 \text{ K}$) [3]. In the latter group, the electrical energy applied to the discharge is mainly delivered to the electrons, which in turn excite by collisions with the molecules of the gas where the discharge is established, thus generating large amounts of reactive oxygen and nitrogen species (RONS) and UV radiation in air or similar gas mixtures [4].

The applications of nonthermal discharges are wide, and in recent years, there has been a growing interest in nonthermal plasmas in (and in contact with) liquids due to their multiple technological applications, encompassing areas such as agriculture, medicine,

nanomaterial deposition and environmental care, among others [5–9]. Within agriculture, one of the emerging applications is the curing of plants and seeds with liquids that have previously been exposed to plasma (referred to as ‘activated’ liquids), such as water treated with nonthermal discharges (plasma ‘activated’ water or PAW) [5]. In terms of environmental care, due to its ability to decompose organic in water, the use of nonthermal plasmas has focused on the degradation of dyes and pigments (e.g., indigo carmine) used in various industrial sectors, which are resistant and refractory to traditional treatment processes and generate serious damage to human health [10,11].

A widely used type of nonthermal discharge in contact with liquids is the pulsed corona discharge. The corona discharge is a nonuniform discharge that occurs in the vicinity of electrodes of small radius of curvature where the electric field is high enough, and therefore the ionization and luminosity of the discharge are located around these electrodes. Depending on the mechanism through which the ionization level of the discharge is sustained, that depends on the polarity of the electrode where the electric field is higher, the corona discharge is classified as (i) positive corona, when the high electric field is located in the vicinity of the anode and the breakdown mechanism is streamer-type; or (ii) negative corona, when the high electric field is located at the cathode and the breakdown mechanism is Townsend-type [4]. The region in the vicinity of the electrode where the electric field is sufficiently high and ionization processes take place is called the active volume of the corona. This is the most important part of the discharge, as this is where most of the reaction and excitation processes occur. However, the power of the quasi-steady-state corona discharges is typically very low and not suitable for many applications. On the other hand, if the voltage applied to the discharge exceeds a certain threshold, the corona discharge may eventually degenerate into the streamer–spark transition, and if external conditions allow it, into an arc. This transition may be a consequence of a thermal instability. One of the ways to avoid the spark transition—also strongly increasing the power of the discharge—is the application of voltage pulses of short duration (~100 ns) and fast rise time, i.e., the pulsed corona discharge [4].

The gas-phase chemistry of air discharges in contact with liquids produces large amounts of gaseous RONS (OH^\cdot , H_2O_2 , O_3 , NO , NO_2) that enter the liquid volume by diffusion and induce the formation of secondary reactive species in the liquid, such as OH^\cdot , H_2O_2 , NO_2^- , NO_3^- , ONOO^- ; and $\text{O}_2^{\cdot-}$ / HO_2^\cdot radicals [12]. However, the most reactive gaseous species (e.g., OH^\cdot and O_3) are consumed rapidly in solution, so the depth of penetration into the liquid is a few hundred nm to tens of μm [13]. Furthermore, the plasma interacts with the liquid surface, generating reactive species directly at the gas–liquid interface [14]. This makes nonthermal plasmas an advanced oxidation technology [15]. Because the interaction between plasma and liquid is essentially concentrated in this boundary layer, a high-level of interaction requires high values of the gas–liquid interface area (e.g., injecting the liquid as an aerosol or thin layers [13,14,16]).

The OH^\cdot radical is of particular importance in plasma discharges in contact with liquids or in humid air. It has a high oxidizing power ($E^0 = 2.85 \text{ V}$), being the strongest oxidant in aqueous environments. It reacts with most organic compounds, and due to its high reactivity, its life time is very short (in the gas phase it lasts close to 200 μs ; and much less in aqueous-phase, ~1 ns) and therefore, it can react with target molecules in its immediate neighborhood [17]. In the gas phase its generation is mainly through the dissociation of H_2O molecules via electron impact or via the quenching of the excited states of N_2 molecules, while in the liquid phase the photodissociation of water and charge-exchange reactions of incident positive ions on the liquid surface are the main pathways. In PAW, other important formation mechanism of OH^\cdot radical in the bulk liquid is through the degradation of peroxinitrous acid ($\text{O}=\text{NOOH}$)—formed by the reaction between H_2O_2 and NO_2^- —in acidic conditions [13].

Pollutant degradation (such as pharmaceuticals, pesticides and organic dyes) in water induced by nonthermal plasma discharges in (and in contact with) liquids has been extensively studied, as summarized in a recent review articles [15,18]. The principal mech-

anism of pollutant degradation is associated with the most reactive species (OH^\cdot , $\text{O}_2^{\cdot-}$, O_3) formed in the gas phase during the discharge, which enter in the liquid bulk, react with the contaminant molecule, and fragment it. However, the results are highly dependent on the configuration of the discharge, as well as how the energy is deposited in the plasma.

In this work, the degradation of indigo carmine (IC) induced by a pulsed positive corona discharge operating in air is reported. Two volumes of IC solution in distilled water (50 and 100 mL) were treated with different plasma exposure times (10–30 min). Discharge and postdischarge effects on the IC degradation and the concentration of long-lived species in the aqueous phase (NO_3^- , NO_2^- and H_2O_2), were investigated up to 24 h after treatment. In addition, a chemical model to explain the IC chromogenic-bond degradation in the postdischarge phase via the $\text{O}=\text{NOOH}$ decomposition was developed. Moreover, for each of these volumes, the energy yield was estimated as the amount of dye degraded per kWh delivered to the discharge (g/kWh).

2. Materials and Methods

2.1. Pulsed Positive Corona Discharge

A (positive) pulsed corona discharge in open air in contact with liquid was used in the experiments. The discharge was powered with a capacitive pulsed source, capable of delivering voltage pulses with a time-width of ~ 100 ns, an amplitude of ~ 10 kV, and a pulse repetition frequency of ~ 42 Hz. The operation of the source is based on the charging of a capacitor bank ($C = 224$ nF) to a voltage level of 1500 V, which is in turn discharged by a thyristor onto a pulse transformer with ferrite core (Figure 1a).

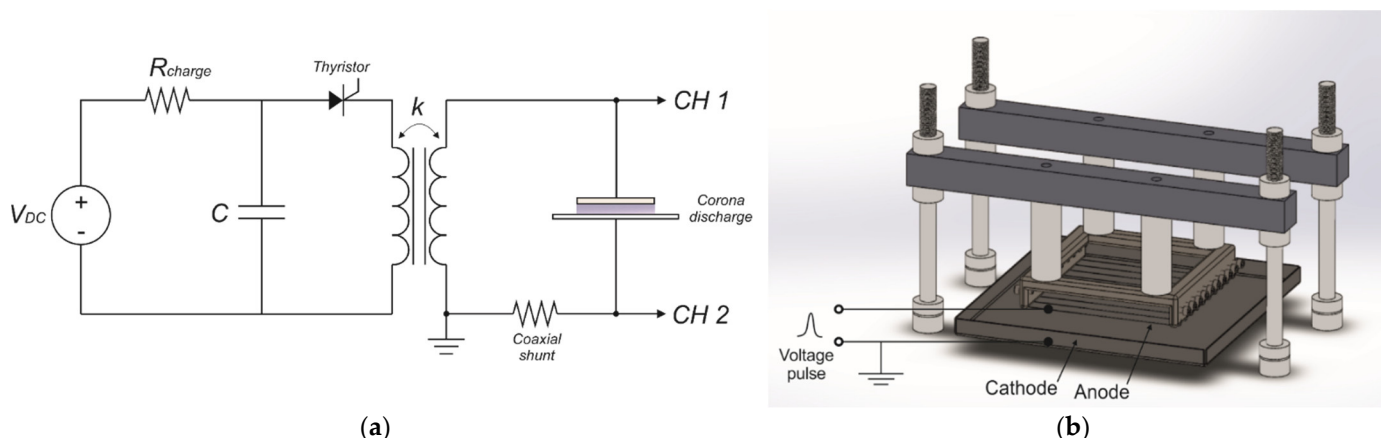


Figure 1. (a) Schematic of the capacitive pulsed source and electrical parameters measurement circuit, (b) schematic of the plasma reactor. The anode consisted of 10 parallel wires spaced 10 mm apart and the cathode consisted of a stainless-steel reservoir containing the liquid in the form of a thin film.

The plasma reactor was set in a wire-to-plate electrode configuration with electrodes made in AISI 304 (Figure 1b). The anode consisted of an arrangement of 10 wires of 0.2 mm in diameter and 100 mm in length with a separation between them 10 mm. These wires were placed parallel and at a certain distance from the cathode, which consisted of a square reservoir with a side of 140 mm and a height of 10 mm, containing the distilled water or IC solution to be treated in the form of a thin layer. Two volumes of the liquid to be analyzed were used: 50 and 100 mL; and in both cases the same gas gap of 3 mm was maintained between the surface of the liquid and the wires that form the anode.

Discharge voltage (V) was obtained as the difference between the CH1 and CH2 voltage signals (Figure 1a). A high-voltage probe (Tektronix P6015A, 1000X, 3 pF, 100 M Ω) was used to measure CH1, while a coaxial shunt resistor (T&M SDN-414-025, 0.25 Ω , 1200 MHz) was used in CH2 to infer the discharge current (I). The signals of both channels were recorded with a 4-channel digital oscilloscope (Tektronix TDS 2004C, sampling rate 1 GS s^{-1} , bandwidth 70 MHz). Due to the difference in length between the measurement

lines (the cable used in CH1 has a length of approximately 3 m, while the corresponding to CH2 has length of 1.5 m) a delay of approximately 10 ns in the voltage signal with respect to the current signal was measured.

Figure 2a shows typical voltage and current waveforms of the discharge for each applied voltage pulse. The voltage pulse reached a maximum value of ≈ 11 kV, while the current pulses reached a maximum near to 30 A, with a time width of ≈ 40 ns.

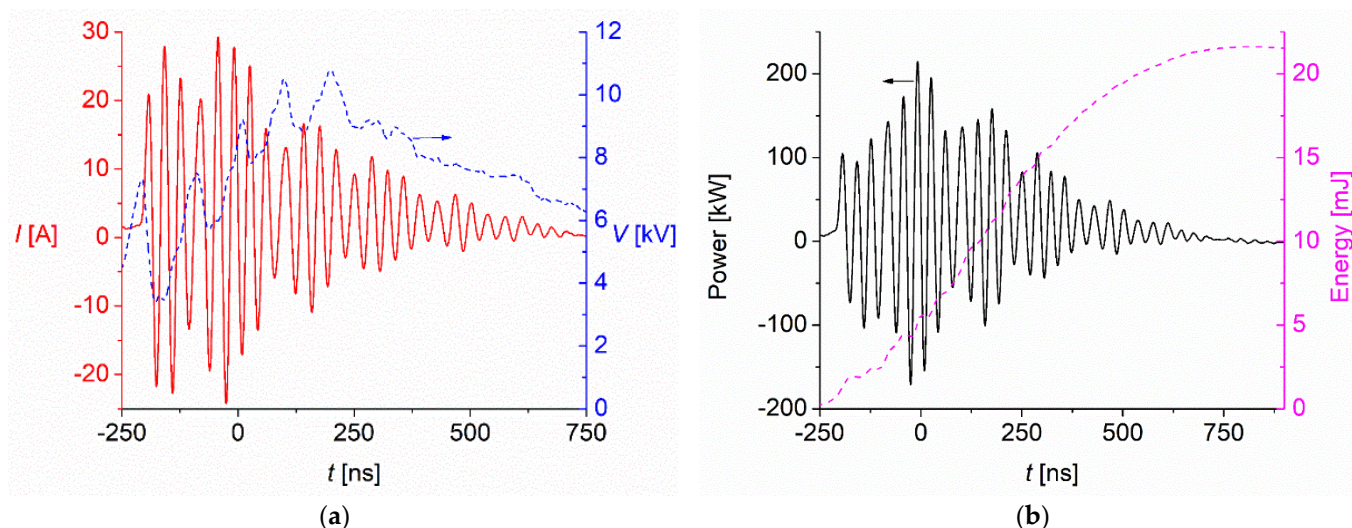


Figure 2. (a) Voltage and current pulse waveforms of the discharge (arrow indicates the voltage scale); (b) instantaneous power and energy dissipated in the discharge (arrow indicates the power scale).

The instantaneous power and energy dissipated in the discharge are shown in Figure 2b. The instantaneous power (the product of $V I$) oscillated with the same frequency as the discharge current, reaching a maximum around 200 kW, while the average power per pulse was ≈ 21 kW. The energy per pulse, calculated as the time integral of the instantaneous power, reached a value of ≈ 21 mJ. Taking into account the pulse repetition frequency, the corresponding mean power resulted at about 0.9 W.

2.2. Treatments and Statistical Analysis

Volumes of 50 and 100 mL of distilled water ($\text{pH} \approx 5.2$ and electrical conductivity $\approx 5 \mu\text{S}/\text{cm}$) or IC solution subjected to different plasma exposure times were studied: 0 (control), 10, 20 and 30 min. Each of these experiments was performed in triplicate. Statistical analyses were performed with the R 4.1.1 software, R Core Team, R Foundation for Statistical Computing (Vienna, Austria) [19]. Data are shown as mean values \pm SEM.

2.3. Physicochemical Determinations

2.3.1. IC Degradation

To study the IC degradation, 50 and 100 mL of a 20 mg/L dye solution (5,5'-Indigo sulfonic acid sodium salt, Cicarelli) were treated with plasma and the absorbance was measured at 285 and 610 nm [10,20] immediately at the end of the treatment and at 24 h after discharge. The treated samples were stored at room temperature in sterile flasks, tightly capped and in the dark for 24 h and the absorbance was remeasured at these wavelengths. The results are shown as percentage degradation of the IC with respect to the initial concentration: $\% = 100 (1 - A/A_0)$, where A is the absorbance of the treated sample and A_0 is the absorbance of the untreated sample.

2.3.2. pH and Electrical Conductivity

The levels of pH and electrical conductivity were determined using a HI 8314 pH meter (Hanna) with a range of 0 to 14 and a resolution of 0.01; and a CYBERSCAN COND 610 conductivity meter (Oakton Instruments, Vernon Hills, IL, USA) with a measurement

range of 0 to 500 mS/cm with an accuracy of 1%. Both instruments were calibrated prior to the determinations using standard solutions (buffer pH 7, buffer pH 4 and KI 0.01 M solution with $\sigma = 1413 \mu\text{S}/\text{cm}$ at 25 °C). The determinations were performed at the end of the plasma treatments.

2.3.3. Hydrogen Peroxide Measurement

A method using peroxidase was used [21]. The method is based on the reaction of H_2O_2 with a mixture of 4-aminophenazone and phenol to give as product a red quinoneimine (4-(p-benzoquinonamonoimino)-phenazone) that exhibits an absorption maximum at 505 nm.

2.3.4. Nitrate Measurement

The UV method was used [21]. Hydrochloric acid was added in a ratio water:HCl = 50:1 and the absorbance at 220 nm (A_{220}) and 275 nm (A_{275}) was measured. These values were used to obtain the corrected absorbance ($A = A_{220} - 2 A_{275}$).

2.3.5. Nitrite Measurement

Nitrite concentration was measured using Griess reagents (I and II) [21]. This technique consists of detecting a color change of the solution to a pink when nitrite react sequentially with sulfanilic acid and α -naphthylamine. After adding the reagents, the sample is allowed to react for 20 min and the absorbance at 520 nm is measured.

At the same time, calibration curves and their respective quality controls were processed for the determination of the reactive species. Using these curves, the concentrations of the compounds in mg/L were calculated. The standards and quality controls were prepared with analytical quality drugs, with known concentrations and within the range of the measured concentrations.

Measurements of the reactive species in activated water were made at the end of the plasma treatment, at 5 h and 24 h after treatment, in order to correlate these concentrations with the results obtained in the IC degradation. The treated samples were stored at room temperature (25 ± 2 °C) in sterile flasks, tightly capped and in the dark.

2.4. Modeling of IC Degradation in the Postdischarge Phase

A chemical model to estimate the degradation rate of the IC chromogenic bond in the postdischarge phase via the $\text{O}=\text{NOOH}$ decomposition was developed. To this end, the value of the third-order rate coefficient for the production of $\text{O}=\text{NOOH}$ under the conditions considered was obtained [22].

3. Results and Discussion

3.1. pH and Electrical Conductivity in PAW

The levels of pH and electrical conductivity of PAW were measured immediately after treatment with plasma. The variation of these variables can be seen in Figure 3. The pH showed a significant decrease from ≈ 5.2 to 3.8 with increasing plasma exposure time and decreasing volume (Two-way ANOVA, $p < 0.05$). The pH variation depends on the type of discharge and gas used. The decrease in the pH of aqueous solutions treated with electrical discharges in air is mostly attributed to the formation of nitric and nitrous acids in solution [17].

The electrical conductivity increased significantly with treatment time for both volumes studied with an approximately linear dependence. For the 50 mL volume, the conductivity reached a significantly higher value, close to double, compared to 100 mL for all plasma exposure times. This is expected due to the higher level of gas-liquid interaction at the interface area in the thinner water layer. The increase in conductivity with plasma exposure time is associated with acidic effects and the formation of NO_2^- and NO_3^- ions in water [17].

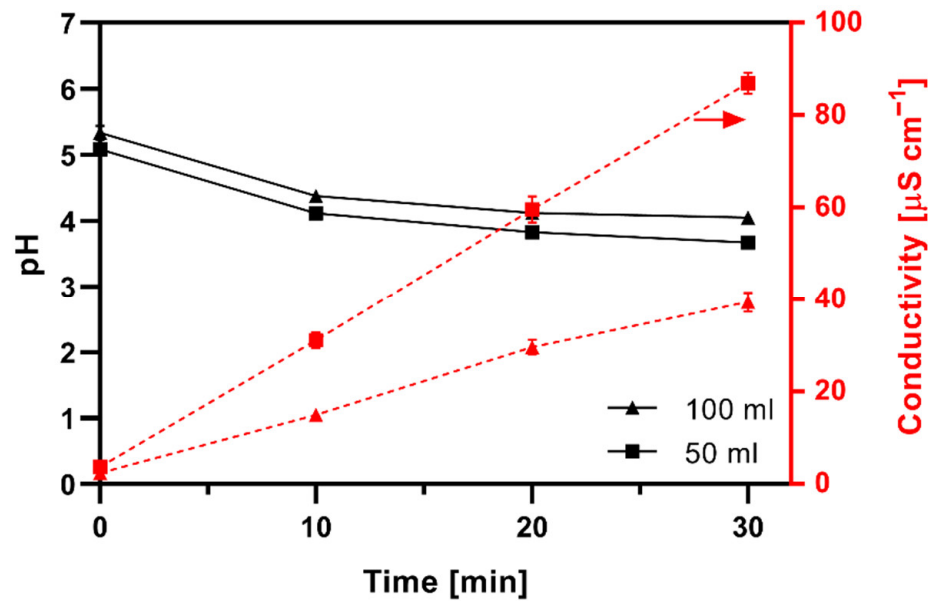


Figure 3. Variation of pH and electrical conductivity of PAW as a function of treatment time (min) with plasma for two sample volumes (50 and 100 mL). Two-way ANOVA, $p < 0.05$.

3.2. Concentration of Reactive Species in PAW

In all cases, reactive species increased significantly with plasma exposure time and with decreasing volume of water (two-way ANOVA, $p < 0.05$) (Figure 4). The increase in the concentration of reactive species as the volume decreases was also documented by other authors [23,24], suggesting that the species responsible for the variation of pH, conductivity and formation of secondary species are formed at the gas-liquid interface and then transferred to the bulk liquid, and that the generation rate of the species does not depend on the treated volume. In plasma-liquid discharges, water evaporation enhances the generation of OH^\cdot and H_2O_2 in the gas phase, which in turn are transported to the plasma-liquid interface based on their solubility coefficients [12], thus promoting the formation of secondary species in the water phase.

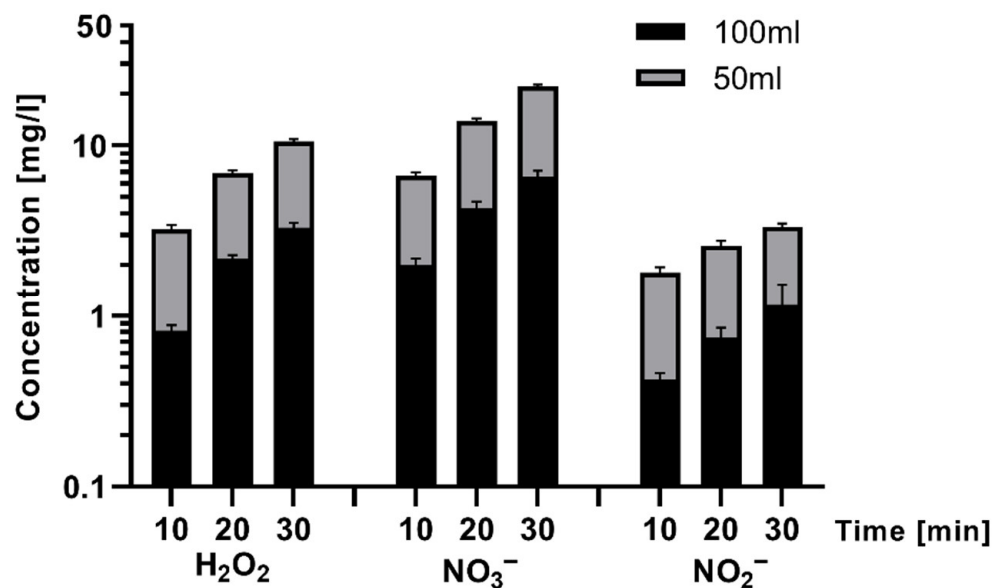


Figure 4. Concentration of the reactive species as a function of treatment time (min) with plasma for two sample volumes (50 and 100 mL). Two-way ANOVA, $p < 0.05$.

3.2.1. Hydrogen Peroxide

H₂O₂ increased significantly with plasma exposure time (Figure 4), reaching a maximum of ≈7.2 mg/L in 50 mL and ≈3.3 mg/L in 100 mL. H₂O₂ formed in the gas phase by the discharge has a high Henry's law solubility coefficient (≈9 × 10⁻² M⁻³ Pa⁻¹), so almost all H₂O₂ (g) rapidly transfers to the liquid bulk [12]. Although H₂O₂ has a relatively high oxidation potential, its direct oxidation effect in water is low because it does not react significantly with most organic compounds. However, this species involves processes that affect water chemistry, including the formation of OH· radicals by reacting with nitrite through the formation of peroxyxynitrous acid [17]. Consequently, this advanced oxidation chemistry generates much more reactive species than H₂O₂; for this reason, nonthermal discharges produce very efficient processes for organic-compound degradation and water disinfection.

3.2.2. Nitrate and Nitrite

NO₃⁻ and NO₂⁻ concentrations increased significantly with plasma exposure time, reaching peak values of ≈15.6 mg/L for NO₃⁻ and ≈2.2 mg/L for NO₂⁻ (Figure 4) in 50 mL, obtaining a ratio of 1:7, similar to that established by other authors in solution [10]. Similar concentrations have been described by other authors using plasma equipment with a voltage of 15 kV and exposure time of 5 min [25].

Nitric oxide (NO) formed through dissociated oxygen and nitrogen in air discharges via the Zeldovich reactions reacts with oxygen or ozone to form nitrogen dioxide (NO₂), which upon dissolving in water leads to the formation of NO₂⁻ and NO₃⁻ ions through electron capture by NO₂ or through oxidation of NO [17]:



In these reactions, it can be clearly seen that the formation of these ions in solution contributes to the drop in pH by the release of H⁺ ions into the water.

3.3. Time Evolution of the Concentration of Reactive Species in the Postdischarge

The stability of the reactive species in PAW up to 24 h after treatment is presented in Figure 5. The results corresponded to 50 mL sample volume treated for 30 min. The NO₃⁻ concentration remained stable for 24 h with a value of 15.7 mg/L immediately after treatment, and 15.5 mg/L after 24 h of storage. Similar results were reported by Vlad et al. [24], who showed that nitrate was also stable in solution for 20 days after treatment.

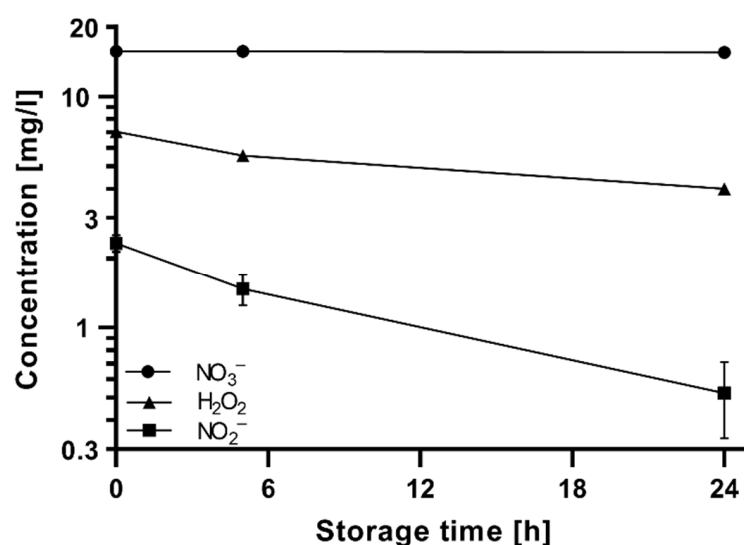
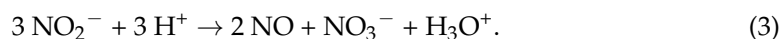


Figure 5. Variation of nitrate (NO₃⁻, mg/L), hydrogen peroxide (H₂O₂, mg/L) and nitrite (NO₂⁻, mg/L) concentrations in PAW at 5 h and 24 h after plasma treatment. One-way ANOVA, *p* < 0.05.

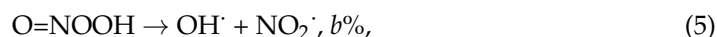
A significant decrease in hydrogen peroxide from 7.1 mg/L to 4 mg/L was observed after 24 h of storage time (Figure 5). Other authors [25,26] have documented decreases in hydrogen peroxide concentration after storage of plasma-treated solutions for 24 h. A significant drop in NO_2^- concentration from 2.3 mg/L to 0.5 mg/L at 24 h was also observed. Previous studies have also reported a significant decrease in nitrite and an increase in nitrate concentration after 48 h [25] or 7 days of storage [26]. The NO_2^- to NO_3^- disproportionation reaction is as follows [17]:



which is strongly pH-dependent and is not expected to be a significant pathway of nitrite loss under the conditions considered (proceeds faster at $\text{pH} < 3.5$). On the other hand, the peroxyxynitrous acid formation is an important pathway by which nitrite and hydrogen peroxide are consumed in the aqueous phase [17]:



Reaction (4) is of particular importance in plasmas in contact with water because of the large amount of H_2O_2 produced in discharges of this type. In acidic solutions, the predominant form of peroxyxynitrite is the protonated form ($\text{p}K_a = 6.8$), which decays to OH^\cdot and NO_2^\cdot radicals via (5), and to NO_3^- via (6), with their corresponding branching values [13]:



b values reported in the literature vary between 0.15 and 0.4 [13]. Although both radicals in reaction (5) can recombine to form nitric acid, the rate constant of that reaction ($>3 \times 10^4 \text{ L mol}^{-1} \text{ s}^{-1}$) is several orders of magnitude lower than most of the rate constants of the destruction OH^\cdot reactions ($10^7 \div 10^{10} \text{ L mol}^{-1} \text{ s}^{-1}$), so the reactivity of peroxyxynitrous acid is determined primarily by the OH^\cdot radicals formed from (5) [17].

3.4. IC Degradation: Discharge and Postdischarge Effects

Indigo carmine degradation immediately after discharge (0 h) increased with both plasma exposure time and decreasing volume (Two-way ANOVA, $p < 0.05$), showing a significant difference between treatments. Maximum values for the degradation of the IC unsaturated bond (measured at 285 nm) at 0 h was obtained for a plasma exposure time of 30 min: 81.3% and 86% for sample volumes of 100 mL and 50 mL, respectively (Figure 6a), while corresponding values for the IC chromogenic bond (measured at 610 nm) at the same plasma exposure time were 93.4% and 99.1%, respectively (Figure 6b). These results can be primarily associated to the diffusion into the liquid of O_3 and OH^\cdot (main oxidizing species for the IC dye [27]) generated in the gas phase through plasma-mediated reactions. It should be noted that due to their short lifetime ($<1 \text{ ns}$), plasma-generated OH^\cdot radicals are not expected to diffuse far beyond a thin boundary layer (of the order of 100 nm to 10 μm) near the gas–liquid interface [13]. As for O_3 , it is worth mentioning that despite its hydrophobicity and low Henry's law diffusion coefficient, the diffusion of O_3 in the liquid volume is favored, since upon entry it reacts with the IC molecule, being rapidly consumed in solution [10].

It is also observed that for low plasma exposure times ($<20 \text{ min}$) the IC degradation of both the chromogenic and unsaturated bonds at 24 h post-treatment was higher than 0 h; with the IC degradation for 50 mL being higher than 100 mL (Figure 6). Such a marked difference in the IC degradation between measurements at 0 h and 24 h post-treatment suggests that the OH^\cdot production in the bulk liquid through the decomposition of the $\text{O}=\text{NOOH}$ pathway (5) plays a major role in the IC degradation in the postdischarge [13]. Moreover, the difference in IC degradation between volumes could be related to a change in the level of the gas–liquid interaction. As quoted before, the concentration of nitrite

and hydrogen peroxide—which increases the availability of OH[•] radicals—significantly increased their concentration at lower volume, leading to more oxidants in solution. However, for higher plasma exposure times, the IC degradation was almost independent of both the volume treated and the post-treatment time, thus indicating that the IC degradation limit was already reached.

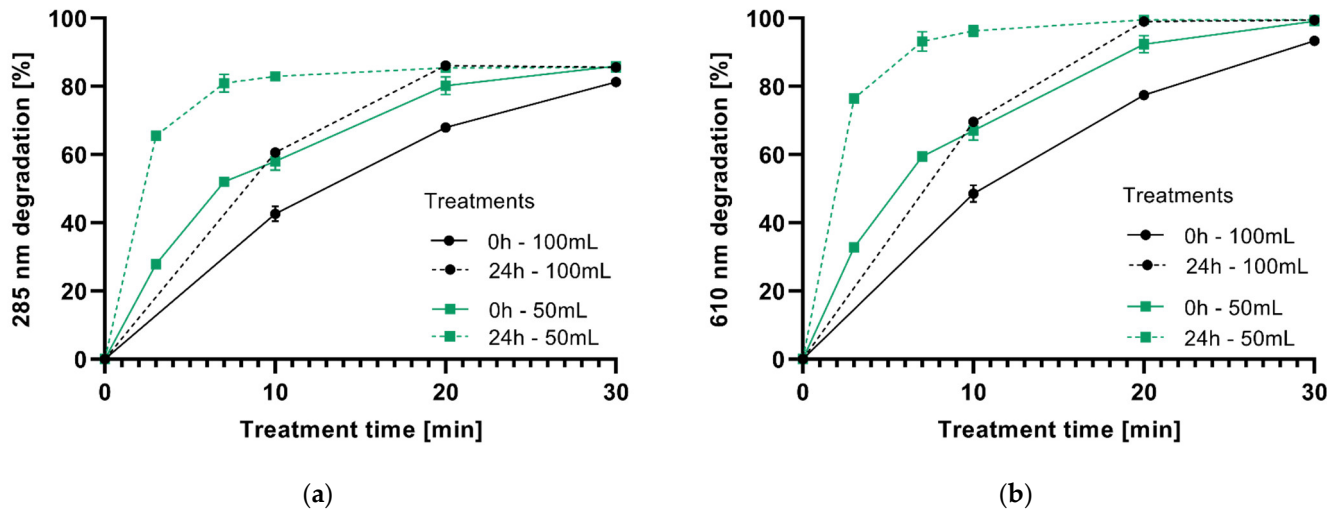


Figure 6. IC degradation immediately after discharge (0 h) and after 24 h of storage (24 h), as a function of treatment time (0–30 min), for two volumes of water (50 and 100 mL) at 285 nm (a) and 610 nm (b).

3.4.1. Modeling of the IC Degradation in the Postdischarge Phase

In the postdischarge phase (i.e., without the generation of reactive species formed in the gas-phase by the plasma) it is reasonable to assume that the IC chromogenic bond degradation is due to the interaction of the dye molecule with the OH[•] radical, formed through the O=NOOH decomposition in the bulk liquid. The O=NOOH is formed via reaction (4) (i.e., NO₂⁻ + H₂O₂ + H⁺ → O=NOOH + H₂O); and quickly decomposes via (5) and (6) [13]. The formation rate of O=NOOH obtained from reaction (4) is as follows:

$$d[\text{O}=\text{NOOH}]/dt = k_4 [\text{NO}_2^-] [\text{H}_2\text{O}_2] [\text{H}^+], \tag{7}$$

where k_4 is the third-order rate coefficient of (4) and [NO₂⁻], [H₂O₂] and [H⁺] are the concentrations of NO₂⁻, H₂O₂ and H⁺, respectively. It is worth noting that estimating the formation rate of O=NOOH (and consequently the formation of OH[•] radicals in solution) necessarily implies knowing the k_4 value, which is pH-dependent. To estimate the k_4 value for the given conditions, the procedure developed by Lukes et al. was followed [22]. Due to the fact that during the postdischarge the pH data remained within a value of 3.87 ± 0.02, the corresponding concentration of H⁺ (=10^{-pH}) was almost constant. Under such conditions, the third-order reaction (7) can be simplified to a pseudo-second-order reaction as

$$d[\text{H}_2\text{O}_2]/dt = -k_4^{SO} [\text{NO}_2^-] [\text{H}_2\text{O}_2], \tag{8}$$

where $k_4^{SO} \equiv k_4 [\text{H}^+]$ is the pseudo-second-order rate constant of reaction (4). Moreover, the rate of O=NOOH formation (7) can be expressed in terms of the rate of disappearance of reactants, as

$$d[\text{O}=\text{NOOH}]/dt = -d[\text{NO}_2^-]/dt = -d[\text{H}_2\text{O}_2]/dt. \tag{9}$$

The integration of (8) and (9) between $t = 0$ and t gives:

$$\ln ([\text{NO}_2^-] [\text{H}_2\text{O}_2]_0) - \ln ([\text{H}_2\text{O}_2] [\text{NO}_2^-]_0) = k_4^{SO} ([\text{NO}_2^-]_0 - [\text{H}_2\text{O}_2]_0) t, \tag{10}$$

where the zero subscript indicates species concentrations at $t = 0$ in the postdischarge. The experimental data for this analysis were used from post-treatment evolution of $[\text{NO}_2^-]$ and $[\text{H}_2\text{O}_2]$ in a sample volume of 50 mL of PAW treated for 20 min (Figure 7a). The plot of (10) as a function of the time together with the corresponding linear fit is presented in Figure 7b.

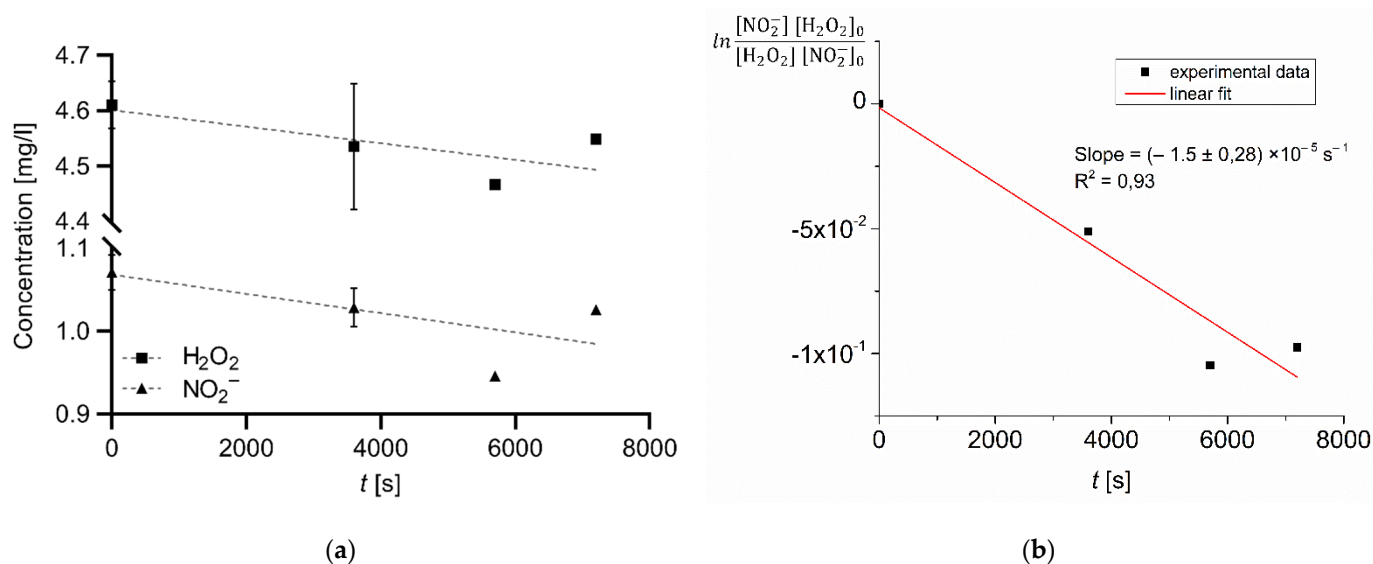
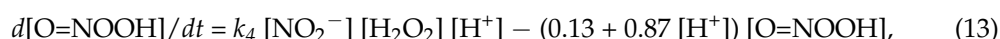


Figure 7. (a) Post-treatment evolution of $[\text{NO}_2^-]$ and $[\text{H}_2\text{O}_2]$ in a sample volume of 50 mL of PAW treated for 20 min (lines are a guide to the eye). (b) Plot of (10) as a function of time.

It is observed in Figure 7b that the experimental data for H_2O_2 and NO_2^- satisfy the expression for the second-order reaction (10), the value of the second-order rate coefficient being determined from the slope k_4^{SO} ($[\text{NO}_2^-]_0 - [\text{H}_2\text{O}_2]_0$). The third-order rate coefficient k_4 was then obtained as $k_4 = k_4^{SO}/[\text{H}^+] = (1075 \pm 200) \text{ M}^{-2} \text{ s}^{-1}$. This value is in very good agreement with that reported by Lukes et al. ($1100 \text{ M}^{-2} \text{ s}^{-1}$ for a pH of 3.3) [22], and Damschen et al. ($1200 \text{ M}^{-2} \text{ s}^{-1}$ for a pH of 3.8) [28].

It is worth noting that as reactions other than the decomposition of $\text{O}=\text{NOOH}$ arising from stable RONS in water (i.e., H_2O_2 , NO_2^- , and NO_3^-) do not significantly oxidize indigo carmine, the measured concentrations of these species in PAW can be used to estimate the corresponding concentrations in IC solution. Measurements of NO_2^- and H_2O_2 in PAW and in IC solution were similar (data not shown). Moreover, as the O_3 would react with indigo carmine almost instantly [13], neglectable concentrations of O_3 in IC solution are expected in the postdischarge.

Once the k_4 value was determined for the given experimental conditions, it is possible to model the IC chromogenic bond degradation related to the $\text{O}=\text{NOOH}$ decomposition based on the following bulk-liquid reactions:



where (11) corresponds to the IC destruction by the OH' radicals, while (12) and (13) correspond to the processes of formation and destruction of OH' radicals and $\text{ONOO}=\text{H}$, respectively.

Since the timescale for the IC degradation under the given conditions (~ 1 h) is very large compared to the lifetimes of OH' and $\text{O}=\text{NOOH}$ (the decomposition rate of $\text{O}=\text{NOOH}$ is $0.13 + 0.87 [\text{H}^+]$, s^{-1} [29]) it is reasonable to assume that such species are in instantaneous

equilibrium (i.e., the accumulation terms in (12) and (13) are taken as zero). Under such assumption, (11) can be rearranged as [13]:

$$d[\text{IC}]/dt = -b k_4 [\text{NO}_2^-]_0 [\text{H}_2\text{O}_2]_0 [\text{H}^+]_0 [\text{IC}]/[\text{IC}]_0, \quad (14)$$

with the branching value b being the parameter of the model. Figure 8 shows the IC degradation yielded by the model for $b = 0.4$, together with experimental data.

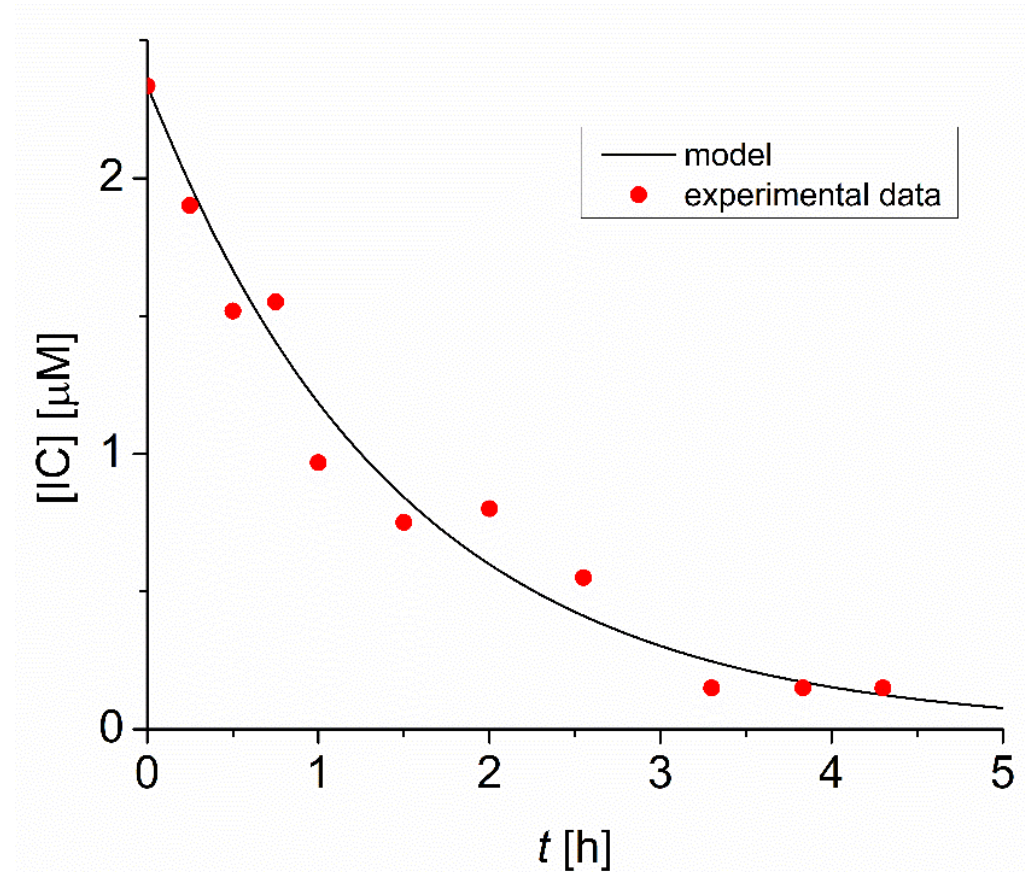


Figure 8. Degradation of the IC chromogenic bond, experimental versus predicted by the model.

The good agreement between the experimental degradation data for the IC chromogenic bond and those obtained through the model (Figure 8) support the hypothesis that during the postdischarge phase, the most important mechanism of IC discoloration is by interaction with the OH^\cdot radical formed in the liquid bulk through the decomposition of $\text{O}=\text{NOOH}$ [13].

3.4.2. Subproducts of the IC Degradation

The degradation of IC in water is a good indicator of the amount of oxygen-based reactive species produced, in particular ozone [30]. The molecule of IC in contact with the reactive species generated by the plasma fragments, leads to the formation of fragmented intermediates, such as isatin-5-sulfonic acid, which gives a yellowish or colorless appearance to the treated solution [30]. One way to corroborate the fragmentation of the IC molecule in isatin-5-sulfonic acid is by measuring the absorbance at 250 nm [10,31] immediately after discharge. Figure 9 shows the significant increase in absorbance at 250 nm for the 50 mL samples of IC treated 30 min.

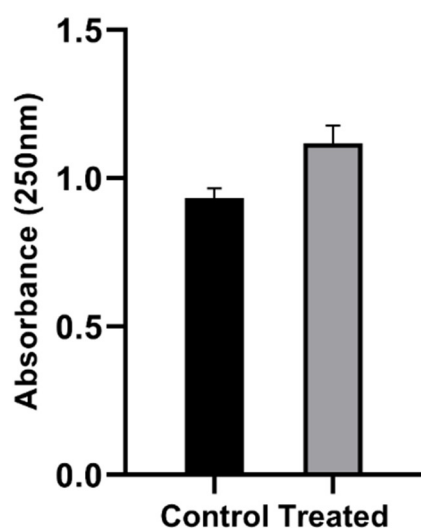


Figure 9. Absorbance at 250 nm of 50 mL samples untreated (Control) and treated with plasma for 30 min (Treated). Student's *t*-test, $p < 0.05$.

3.5. Energy Yield G_{50}

The energy yield G_{50} of the discharge was determined as the ratio between the amount of the converted IC and the energy required for 50% IC conversion: $G_{50} = 1.8 \times 10^6 C_0 V_0 M_0 / (P t_{50})$ [g/kWh], where C_0 is the molar concentration of the control IC, V_0 is the treated volume in liters, M_0 is the molecular weight of the IC in grams, P is the average power of the plasma reactor in watts, and t_{50} is the time in seconds required for 50% conversion [16]. Although the G_{50} value is usually calculated at 0 h, its calculation at 24 h becomes relevant if the treated liquid is not used immediately, having a storage time of at least 1 day. The G_{50} values obtained at 0 h and 24 h post-treatment are shown in Table 1.

Table 1. Energy yield G_{50} for 50 mL and 100 mL of IC solution calculated at 285 nm and 610 nm at 0 h and 24 h post-treatment.

Post-Treatment Time	G_{50} [g/kWh]			
	(at 285 nm)		(at 610 nm)	
	50 mL	100 mL	50 mL	100 mL
0 h	5.2	5.2	6	6.2
24 h	15.5	8.5	17	9.6

Table 1 shows that regardless of the volume of the sample, the energy yield G_{50} values calculated at 0 h are almost constant, with a value of around 5 and 6 g/kWh for the unsaturated and chromogenic bonds, respectively, indicating that the ratios t_{50}/V_0 are remarkably constant under the present conditions. These dependences are strengthened by the fact that in the discharge phase both O_3 and OH^\cdot are mainly formed in the gas phase through plasma-mediated reactions and then transferred to the liquid by diffusion; and that the generation rate of species does not depend on the sample volume. (Note that the rate of degradation through the $O=NOOH$ pathway is dependent on the bulk concentrations of H_2O_2 and NO_2^- and thus changes with sample volume.) On the other hand, the energy yield G_{50} values calculated at 24 h postdischarge decrease noticeably as the sample volume increases. This result is related to the higher concentration of NO_2^- and H_2O_2 in aqueous phase at the lower volume, which in turn increases the availability of OH^\cdot radicals in the liquid bulk through the pathway (5). It is also worth noting that large increases in the energy yield values are observed at 24 h post-treatment due to the beneficial effects induced by the $O=NOOH$ decomposition. For instance, the energy yield G_{50} for the degradation of the unsaturated bond calculated at 24 h and for the 50 mL volume is higher than that

corresponding to 0 h by a factor of about 3. Obtained G_{50} values are in between typical energy-yield values reported for the IC degradation by pulsed corona discharges in contact with water, ranging from 0.149 g/kWh to 294 g/kWh [16].

4. Conclusions

The degradation of indigo carmine (IC) in water induced by a pulsed positive corona discharge (pulse energy of 21 mJ at a repetition rate of 42 Hz) operating in ambient air was investigated. Degradation levels of two different volumes (50 and 100 mL) of IC in solution with distilled water treated with different plasma exposure times (10–30 min) immediately after discharge (0 h), and after 24 h were examined. The results show that:

1. The OH^\cdot radical plays a primary role in the IC degradation. While both O_3 and OH^\cdot contribute to the IC degradation in the discharge phase, the OH^\cdot radical contributes in the postdischarge phase. While both O_3 and OH^\cdot are mainly generated in the gas phase and then transferred to the liquid in the discharge phase, the OH^\cdot radical is mainly produced through the $\text{O}=\text{NOOH}$ decomposition in the postdischarge phase. Noticeably, increases in the energy yield values are observed at 24 h post-treatment due to the beneficial effects induced by the $\text{O}=\text{NOOH}$ decomposition.
2. Maximum values for the degradation of the IC unsaturated bond at 0 h were obtained for a plasma exposure time of 30 min: 81.3% and 86% for sample volumes of 100 mL and 50 mL, respectively; while corresponding values for the IC chromogenic bond at the same plasma exposure time were 93.4% and 99.1% for sample volumes of 100 mL and 50 mL, respectively.
3. For low plasma exposure times (<20 min) the IC degradation of both the chromogenic and unsaturated bonds at 24 h post-treatment was higher than 0 h; being the IC degradation for 50 mL higher than 100 mL. However, for higher plasma exposure times the IC degradation was almost independent of both the volume treated and the post-treatment time.
4. Concentrations of reactive species in the aqueous phase at 0 h increased with the plasma exposure time and decreased with increasing sample volume. The maximum values reached being 7.25 mg/L for H_2O_2 , 15 mg/L for NO_3^- and 2 mg/L for NO_2^- . While the concentrations of NO_2^- and H_2O_2 decreased with post-treatment time, the NO_3^- concentration remained stable.

Author Contributions: Conceptualization, M.G.F., B.L.F. and L.P.; methodology, M.G.F., B.L.F., N.J.M., J.C.C., B.S. and L.P.; software, M.G.F., B.L.F. and B.S.; validation, M.G.F., B.L.F., L.P. and B.S.; formal analysis, B.L.F., M.G.F. and L.P.; investigation, M.G.F., B.L.F. and L.P.; resources, N.J.M.; data curation, B.L.F., B.S. and M.G.F.; writing—original draft preparation, M.G.F. and B.L.F.; writing—review and editing, M.G.F., B.L.F., L.P. and K.B.; visualization, M.G.F. and B.L.F.; supervision, L.P., B.L.F. and K.B.; project administration, L.P., K.B. and B.L.F.; funding acquisition, L.P., K.B. and B.L.F. All authors have read and agreed to the published version of the manuscript.

Funding: This research was funded by Universidad Tecnológica Nacional, grant PID 5447 and PID 5418, Agencia Nacional de Promoción Científica y Tecnológica, grant PICT 2018-00702, CONICET, grant PIP 11220200100459CO, and Agencia Santafesina de Ciencia, Tecnología e Innovación, grant DTT-2021-028.

Institutional Review Board Statement: Not applicable.

Informed Consent Statement: Not applicable.

Data Availability Statement: The data that support the findings of this study are available within the article.

Acknowledgments: M.F. and B.S. thanks CONICET for his doctoral fellowship. J.C.C. thanks CONICET for his postdoctoral fellowship. B.L.F., K.B. and L.P. are members of CONICET.

Conflicts of Interest: The authors declare no conflict of interest. The funders had no role in the design of the study; in the collection, analyses, or interpretation of data; in the writing of the manuscript; or in the decision to publish the results.

References

1. Chen, F.F. *Erratum to: Introduction to Plasma Physics and Controlled Fusion*, 3rd ed.; Springer International Publishing: Los Angeles, CA, USA, 2018; ISBN 9783319223087.
2. Raizer, Y.P. *Gas Discharge Physics*, 1st ed.; Allen, J.E., Ed.; Springer: Berlin/Heidelberg, Germany, 1991; ISBN 978-3-642-64760-4.
3. Boulos, M.I.; Fauchais, P.; Pfender, E. *Thermal Plasmas: Fundamentals and Applications*, 1st ed.; Springer: New York, NY, USA, 1994; ISBN 9781489913395.
4. Fridman, A.; Chirokov, A.; Gutsol, A. Non-thermal atmospheric pressure discharges. *J. Phys. D Appl. Phys.* **2005**, *38*, R1–R24. [[CrossRef](#)]
5. Adamovich, I.; Baalrud, S.D.; Bogaerts, A.; Bruggeman, P.J.; Cappelli, M.; Colombo, V.; Czarnetzki, U.; Ebert, U.; Eden, J.G.; Favia, P.; et al. The 2017 Plasma Roadmap: Low temperature plasma science and technology. *J. Phys. D Appl. Phys.* **2017**, *50*, 323001. [[CrossRef](#)]
6. Wright, K. *Study of Plasma Treatment of Produced Water from Oil and Gas Exploration*; Drexel University: Philadelphia, PA, USA, 2015.
7. Cho, Y.I.; Wright, K.C.; Kim, H.S.; Cho, D.J.; Rabinovich, A.; Fridman, A. Stretched arc discharge in produced water. *Rev. Sci. Instrum.* **2015**, *86*, 013501. [[CrossRef](#)] [[PubMed](#)]
8. Manakhov, A.; Orlov, M.; Grokhovskiy, V.; Alghunaimi, F.I.; Ayirala, S. Functionalized Nanomembranes and Plasma Technologies for Produced Water Treatment: A Review. *Polymers* **2022**, *14*, 1785. [[CrossRef](#)]
9. Choi, S.; Watanabe, T. Decomposition of 1-decanol emulsion by water thermal plasma jet. *IEEE Trans. Plasma Sci.* **2012**, *40*, 2831–2836. [[CrossRef](#)]
10. Crema, A.P.S.; Piazza Borges, L.D.; Micke, G.A.; Debacher, N.A. Degradation of indigo carmine in water induced by non-thermal plasma, ozone and hydrogen peroxide: A comparative study and by-product identification. *Chemosphere* **2020**, *244*, 125502. [[CrossRef](#)]
11. Wright, K. Plasma Water Treatment and Oxidation of Organic Matter in Water. In Proceedings of the IEEE International Pulsed Power Conference, Orlando, FL, USA, 23–29 June 2019; IEEE: Piscataway, NJ, USA, 2019; pp. 35–38.
12. Machala, Z.; Tarabová, B.; Sersenová, D.; Janda, M.; Hensel, K. Chemical and antibacterial effects of plasma activated water: Correlation with gaseous and aqueous reactive oxygen and nitrogen species, plasma sources and air flow conditions. *J. Phys. D Appl. Phys.* **2019**, *52*, 034002. [[CrossRef](#)]
13. Anderson, C.E.; Cha, N.R.; Lindsay, A.D.; Clark, D.S.; Graves, D.B. The Role of Interfacial Reactions in Determining Plasma–Liquid Chemistry. *Plasma Chem. Plasma Process* **2016**, *36*, 1393–1415. [[CrossRef](#)]
14. Foster, J.E. Plasma-based water purification: Challenges and prospects for the future. *Phys. Plasmas* **2017**, *24*, 055501. [[CrossRef](#)]
15. Bruggeman, P.J.; Kushner, M.J.; Locke, B.R.; Gardeniers, J.G.E.; Graham, W.G.; Graves, D.B.; Hofman-Caris, R.C.H.M.; Maric, D.; Reid, J.P.; Ceriani, E.; et al. Plasma-liquid interactions: A review and roadmap. *Plasma Sources Sci. Technol.* **2016**, *25*, 053002. [[CrossRef](#)]
16. Malik, M.A. Water purification by plasmas: Which reactors are most energy efficient? *Plasma Chem. Plasma Process* **2010**, *30*, 21–31. [[CrossRef](#)]
17. Lukes, P.; Locke, B.R.; Brisset, J.L. Aqueous-Phase Chemistry of Electrical Discharge Plasma in Water and in Gas-Liquid Environments. In *Plasma Chemistry and Catalysis in Gases and Liquids*; Parvulescu, V.I., Magureanu, M., Lukes, P., Eds.; 2012; pp. 243–308. ISBN 9783527330065.
18. Kumar, A.; Škoro, N.; Gernjak, W.; Puač, N. Cold atmospheric plasma technology for removal of organic micropollutants from wastewater—A review. *Eur. Phys. J. D* **2021**, *75*, 283. [[CrossRef](#)]
19. R Core Team. *R: A Language and Environment for Statistical Computing*; R Core Team: Vienna, Austria, 2021.
20. Jin, G.; Li, Y.; Fangchuan, Z.; Pingdao, G. Degradation of dye wastewater by ns-Pulse dbd plasma. *Plasma Sci. Technol.* **2013**, *15*, 928–934. [[CrossRef](#)]
21. Baird, R.B.; Eaton, A.D.; Rice, E.W. *Standard Methods for the Examination of Water and Wastewater*, 23rd ed.; Baird, R.B., Eaton, A.D., Rice, E.W., Eds.; American Water Works Association; American Public Works Association; Water Environment Federation: Washington, DC, USA, 2017; ISBN 9780123821652.
22. Lukes, P.; Dolezalova, E.; Sisrova, I.; Clupek, M. Aqueous-phase chemistry and bactericidal effects from an air discharge plasma in contact with water: Evidence for the formation of peroxyxynitrite through a pseudo-second-order post-discharge reaction of H₂O₂ and HNO₂. *Plasma Sources Sci. Technol.* **2014**, *23*, 015019. [[CrossRef](#)]
23. Julák, J.; Scholtz, V.; Kotúčová, S.; Janoušková, O. The persistent microbicidal effect in water exposed to the corona discharge. *Phys. Med.* **2012**, *28*, 230–239. [[CrossRef](#)] [[PubMed](#)]
24. Vlad, I.E.; Anghel, S.D. Time stability of water activated by different on-liquid atmospheric pressure plasmas. *J. Electrostat.* **2017**, *87*, 284–292. [[CrossRef](#)]
25. Zhao, Y.M.; Ojha, S.; Burgess, C.M.; Sun, D.W.; Tiwari, B.K. Inactivation efficacy and mechanisms of plasma activated water on bacteria in planktonic state. *J. Appl. Microbiol.* **2020**, *129*, 1248–1260. [[CrossRef](#)]

26. Traylor, M.J.; Pavlovich, M.J.; Karim, S.; Hait, P.; Sakiyama, Y.; Clark, D.S.; Graves, D.B. Long-term antibacterial efficacy of air plasma-activated water. *J. Phys. D Appl. Phys.* **2011**, *44*, 3–7. [[CrossRef](#)]
27. Minamitani, Y.; Shoji, S.; Ohba, Y.; Higashiyama, Y. Decomposition of dye in water solution by pulsed power discharge in a water droplet spray. *IEEE Trans. Plasma Sci.* **2008**, *36*, 2586–2591. [[CrossRef](#)]
28. Damschen, D.E.; Martin, L.R. Aqueous aerosol oxidation of nitrous acid by O₂, O₃ AND H₂O₂. *Atmos. Environ.* **1983**, *17*, 2005–2011. [[CrossRef](#)]
29. Saha, A.; Goldstein, S.; Cabelli, D.; Czapski, G. Determination of optimal conditions for synthesis of peroxyxynitrite by mixing acidified hydrogen peroxide with nitrite. *Free Radic. Biol. Med.* **1998**, *24*, 653–659. [[CrossRef](#)]
30. Schönekerl, S.; Weigert, A.; Uhlig, S.; Wellner, K.; Pörschke, R.; Pfefferkorn, C.; Backhaus, K.; Lerch, A. Evaluating the performance of a lab-scale water treatment plant using non-thermal plasma technology. *Water* **2020**, *12*, 1956. [[CrossRef](#)]
31. Cano, M.; Solis, M.; Diaz, J.; Solis, A.; Loera, O.; Teutli, M.M. Biotransformation of indigo carmine to isatin sulfonic acid by lyophilized mycelia from *trametes versicolor*. *Afr. J. Biotechnol.* **2011**, *10*, 12224–12231. [[CrossRef](#)]